Bioorganic Chemistry xxx (xxxx) xxx

Contents lists available at ScienceDirect

Bioorganic Chemistry

journal homepage: www.elsevier.com/locate/bioorg

The relationship between stereochemical and both, pharmacological and ADME-Tox, properties of the potent hydantoin 5-HT$_7$R antagonist MF-8

Katarzyna Kucwaj-Brysz [a,1], Gniewomir Latacz [a,1], Sabina Podlewska [a,b], Ewa Żesławska [c], Jarosław Handzlik [d], Annamaria Lubelska [a], Grzegorz Satała [b], Wojciech Nitek [e], Jadwiga Handzlik [a,*]

[a] Department of Technology and Biotechnology of Drugs, Jagiellonian University Medical College, Medyczna 9, 30-688 Kraków, Poland
[b] Maj Institute of Pharmacology, Polish Academy of Sciences, Smętna 12, 31-343 Kraków, Poland
[c] Institute of Biology, Pedagogical University of Cracow, Podchorążych 2, 30-084 Kraków, Poland
[d] Faculty of Chemical Engineering and Technology, Cracow University of Technology, Warszawska 24, 31-155 Kraków, Poland
[e] Faculty of Chemistry, Jagiellonian University, Gronostajowa 2, 30-387 Kraków, Poland

ARTICLE INFO

Keywords:
Serotonin receptors
5-HT$_7$R ligands
Hydantoin
Arylpiperazine
Stereoisomers
DFT
Docking
ADMET

ABSTRACT

This study concerns synthesis and evaluation of pharmacodynamic and pharmacokinetic profile for all four stereoisomers of **MF-8** (5-(4-fluorophenyl)-3-(2-hydroxy-3-(4-(2-methoxyphenyl)piperazin-1-yl)propyl)-5-methylimidazolidine-2,4-dione), the previously described, highly potent 5-HT$_7$R ligand with antidepressant activity on mice. The combination of DFT calculations of ^{1}H NMR chemical shifts with docking and dynamic simulations, in comparison to experimental screening results, provided prediction of the configuration for one of two present stereogenic centers. The experimental data for stereoisomers (**MF-8A-MF-8D**) confirmed the significant impact of stereochemistry on both, 5-HT$_7$R affinity and antagonistic action, with K_i and K_b values in the range of 3–366 nM and 0.024–99 μM, respectively. We also indicated the stereochemistry-dependent influence of the tested compounds on P-glycoprotein efflux, absorption in Caco-2 model, metabolic pathway as well as CYP3A4 and CYP2C9 activities.

1. Introduction

Serotonin 5-HT$_7$ receptor (5-HT$_7$R) is one of the latest discovered subtype from 14-membered serotoninergic system family and is distributed within both central nervous system (CNS) and peripheral tissues [1–3]. The 5-HT$_7$R may couple to G$_s$ protein (increase of cAMP level) or to G$_{12}$ (Rho signaling) [4]. It is attractive therapeutic target since confirmation of its significant role in pathophysiological processes such as depression [5], cognitive impairment, migraines. Despite the fact that there are many approved drugs which interact with 5-HT$_7$R, there is no substance on pharmaceutical market which is highly selective for this receptor [4]. Only one such compound – JNJ-18308683 has been submitted to clinical trials and is being now evaluated in Phase 2 [6,7].

On the other hand, stereochemistry is highly important issue in medicinal chemistry due to possible significant differences in pharmacodynamic and pharmacokinetic properties of particular stereoisomers, which may interact in different ways with many proteins *in vivo* [8–10]. Among ADME-Tox properties affected by compounds chirality, absorption (the difference in binding to the efflux pumps and up-take transporters), metabolism (the difference in orientation to the enzymes reactive moiety), distribution (the difference in binding to the plasma protein) and toxicity (the difference in binding to the hERG channels and in interaction with CYPs) can be mentioned [10]. Especially, the chirality may significantly influence the compounds metabolic stability, which is an important parameter responsible for pharmacokinetic and pharmacological properties. The enantiospecific metabolism was determined for many drugs. For instance, the intrinsic clearance of omeprazole metabolized by CYP3A4 to sulfone metabolite was found in human liver microsomes as around 4-fold greater for the *S*- than for the *R*- enantiomer [11]. The *S*-enantiomer of racemic anticonvulsant drug mephenytoin is oxidized to 4′-hydroxymephenytoin by CYP2C19, whereas the *R*-enantiomer is *N*-dealkylated by two CYPs: 2C9 and 2B6 to

* Corresponding author.
E-mail address: j.handzlik@uj.edu.pl (J. Handzlik).
[1] These authors contributed equally to this work.

https://doi.org/10.1016/j.bioorg.2020.104466
Received 4 December 2019; Received in revised form 30 September 2020; Accepted 6 November 2020
Available online 10 November 2020

phenylethylhydantoin [12,13]. The calcium channel blocker, verapamil, used as a racemic mixture, has shown differences between the plasma concentrations of particular enantiomers. After oral administration, the *S*-isomer has been preferentially metabolized leading to the predominance of *R*-verapamil in plasma [14]. The chiral antidepressant drug, fluoxetine, is an example of the relationship between the genotype and stereoselectivity of metabolism. In extensive metabolizers of CYP2D6, both enantiomers are biotransformed equally to the active metabolite norfluoxetine with similar apparent oral clearances. In CYP2D6 poor metabolizers, however, the apparent oral clearance of *R*-enantiomer is 6-fold higher than that of *S*-fluoxetine. Moreover, the plasma concentration of *S*-fluoxetine is 11.5-fold higher in poor metabolizers than in the extensive ones, whereas only 2.5-fold higher in the case of the *R*-isomer [15].

Recent lines of evidence have indicated a significant influence of stereochemical properties on the compounds' affinity towards 5-HT$_7$R. Among newly synthesized derivatives of pyrrolidone, enantiomers *S* showed much higher potency than enantiomers *R* (Fig. 1) [16].

Results of the studies among the antipsychotic benzamides, *i.e. N*-methylated derivatives of amisulpride (Fig. 2) have indicated a polypharmacologic action of the racemate LB-102, going *via* 5-HT$_7$R (antidepressant effect) and dopaminergic D$_2$ and D$_3$ receptors (antipsychotic activity), whereas radioligand binding assays for corresponding optically pure enantiomers showed that only enantiomer *R* is responsible for interaction with 5-HT$_7$R (Fig. 2) [17]. Taking into account the aforementioned importance of enantioselectivity for both pharmacological and "drug-likeness" properties, it is obligatory to isolate enantiopure components of active racemic mixtures in order to examine them as early as possible in the primary levels of drug discovery process. However, it is usually a great scientific challenge due to sophisticated and expensive stereoselective synthesis methods or even more expensive technics of direct separation of stereoisomers. Furthermore, while the methods of experimental assessment of enantiomeric purity are well developed, available and reliable, a determination of absolute configuration generates many problems. It is an issue strongly determined by the structure and chemical properties of a given molecule, requiring the use of sophisticated spectroscopic methods and/or advanced computer-based prediction techniques, and frequently, it is even impossible to solve without appropriate crystallographic analysis. Thus, usually racemic mixture are under consideration in the first step of drug discovery screening, and only limited "hits" with the desired pharmacodynamic profile are destined to isolate/synthesize their enantiopure components in order to re-evaluate their biological activity and ADME-Tox properties, and thus, to eliminate the inactive, toxic and/or metabolically unstable stereoisomer.

In this context, our previous work [18–21] concerned above 50-membered 5-HT$_7$R hydantoin ligands family, which has been mentioned as recent "breakthrough in medicinal chemistry of novel and powerful antidepressant" by Mangoni *et al.*[22]. The most active member, named **MF-8** (Fig. 3), showed excellent antidepressant effects in forced swim test (FST) in mice at the dose of 5 mg/kg and very profitable ADME-Tox profile [23]. Due to the presence of two stereogenic centers in the structure and achiral synthesis conditions applied in those initial studies [18], **MF-8** was evaluated as a mixture of four possible stereoisomers (**MF-8*rac***).

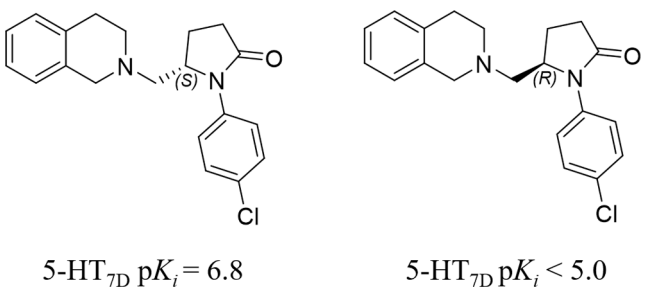

Fig. 1. Differences in 5-HT$_7$ affinity depending on configuration among pyrrolidone derivatives [16].

Based on the very promising biological results, compound **MF-8** was selected for further investigation in term to synthesize and evaluate both, pharmacological and ADME-Tox properties, for each stereoisomer separately. Hence, the current studies are concentrated on the stereoselective synthesis, separation and both, X-ray and molecular modeling-supported, estimation of an absolute configuration of 4 enantiopure stereoisomers of **MF-8**. The obtained stereoisomers have been investigated *in vitro* on their 5-HT$_7$/5-HT$_{1A}$ affinity, 5-HT$_7$ intrinsic activity, passive transport through the biological membranes, absorption in Caco-2 cell-based model, influence on P-glycoprotein (P-gp) activity, metabolic stability, drug-drug interactions (DDI) and hepatotoxicity. Results of corresponding studies for the previously synthesized racemic **MF-8*rac*** [18,19,23] were used for comparison and discussion.

2. Results and discussions

2.1. Chemical synthesis

The particular stereoisomers of **MF-8*rac*** were synthesized *via* already optimized and described 3-step synthetic pathway (Bucherer-Berg reaction, *N*-alkylation and condensation with epoxide ring opening) [19,20] (Scheme 1).

For *N*-alkylation reaction, 2-(chloromethyl)oxirane (epichlorhydrin) with defined configuration was used. The synthesized two pairs of diastereoisomers were separated, after the final step using supercritical fluid chromatography (SFC) technique, with resulting diastereoisomeric excess 92–100% (Table 1). The optically pure stereoisomers with unknown configuration at C5 of hydantoin were assigned with formal signatures A-D used for further investigations.

2.2. Estimation of absolute configuration

The expensive and sophisticated methods of obtaining the stereoisomers (**MF-8A-MF-8D**) provided them in the small amount that enabled to perform only basic spectral and chromatographic analyses, which were not sufficient to recognize the absolute configuration of each final product. Thus, DFT-aided molecular modeling calculations, based on experimental crystallographic data for the racemic mixture of **MF-8**, have been involved to support the ^{1}H NMR spectral analysis in order to estimate the most probable absolute configuration for the stereoisomers **MF-8A-MF-8D**.

2.2.1. X-ray crystal structure analysis for *MF-8*

The chemical group of arylpiperazine 2-hydroxypropyl derivatives of 5-aryl-5-methylhydantoins is hard to obtain in basic precipitate forms, in particular, to have crystals enough for X-ray analysis. In the case of the stereoisomers isolated (**MF-8A-MF-8D**), neither the solid form of them, nor their amount, were sufficient to perform crystallographic studies. In contrary, our 3-year efforts allowed to obtain a crystal of hydrochloride salt form coming from **MF-8*rac***, appropriate for X-ray crystallographic analysis that was a cornerstone for wider structural consideration, carried out by the use of molecular modeling.

Results of the crystallographic studies show that the asymmetric unit consists of one protonated **MF-8** molecule, one chlorine anion and one disordered 2-methylpropan-1-ol molecule, which comes from the solvent. The molecular geometry in the crystal structure of **MF-8** with the atom numbering scheme is shown in Fig. 4.

The molecule possesses two chiral centers at C5 and C7 atoms. The crystal structure confirms 5*S*, 7*S* configuration for one molecule and 5*R*, 7*R* for the other one related by the inversion centers. The molecule of **MF-8** is protonated at nitrogen atom (N2) by the proton transfer from hydrochloride. The linker between hydantoin and piperazine rings adopts extended conformation with torsion angles N3-C6-C7-C8 =

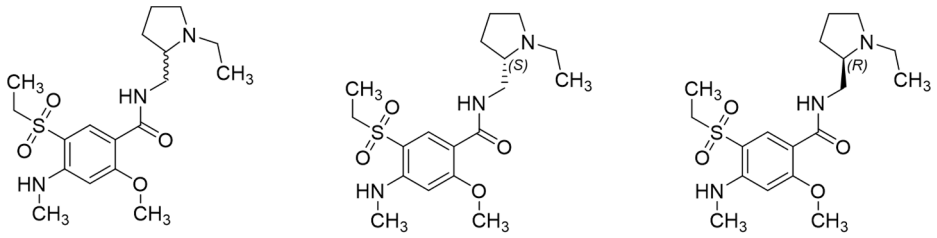

Fig. 2. The differences in pharmacodynamic profile depending on stereochemistry for *N*-methylated amisulpride [17].

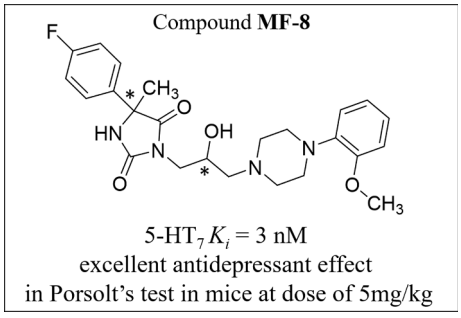

Fig. 3. The structure of **MF-8** with indicated stereogenic centers, 5-HT_7 affinity and *in vivo* activity.

-176.0(1)° and C6-C7-C8-N2 = 168.3(1)°. The molecular structure is stabilized by two intramolecular hydrogen bonds, namely C9-H9A···O1 and C10-H10B···O3. A similar intramolecular interaction of hydroxy group with piperazine ring has been also observed in other crystal structures containing the same linker between hydantoin and piperazine rings [20,21]. The mutual orientation of 4-fluorophenyl substituent at C5 and hydantoin ring is similar to another derivative containing 4-fluorophenyl substituent at C5 atom, for which we determined the crystal structure earlier [21]. The angle between the planes of the aromatic ring and the hydantoin ring is 62.9(1)°, while in the compared compound is 62.2(1)°. In the presented structure the piperazine ring adopts chair conformation with equatorial location of substituents at N2 and N4. The torsion angles C14-C13-N4-C10 and C18-C13-N4-C10 are 71.4(2)° and −110.4(2)°, respectively, which indicate that the phenyl ring at N4 atom is not coplanar with piperazine moiety. The angle between the planes of aromatic and piperazine (C9, C10, C11, C12) rings is 45.8(1)°. Similar values have been observed in other crystal structures of hydantoin derivative containing *o*-metoxyphenyl substituent at nitrogen atom of piperazine ring [24] and similar angles are very often noticed in other crystal structures, deposited in the Cambridge Structural Database, for derivatives containing *o*-metoxyphenyl substituent at nitrogen atom of piperazine ring [25].

The main intermolecular interactions are based on O—H···Cl and N—H···Cl hydrogen bonds (Fig. 5).

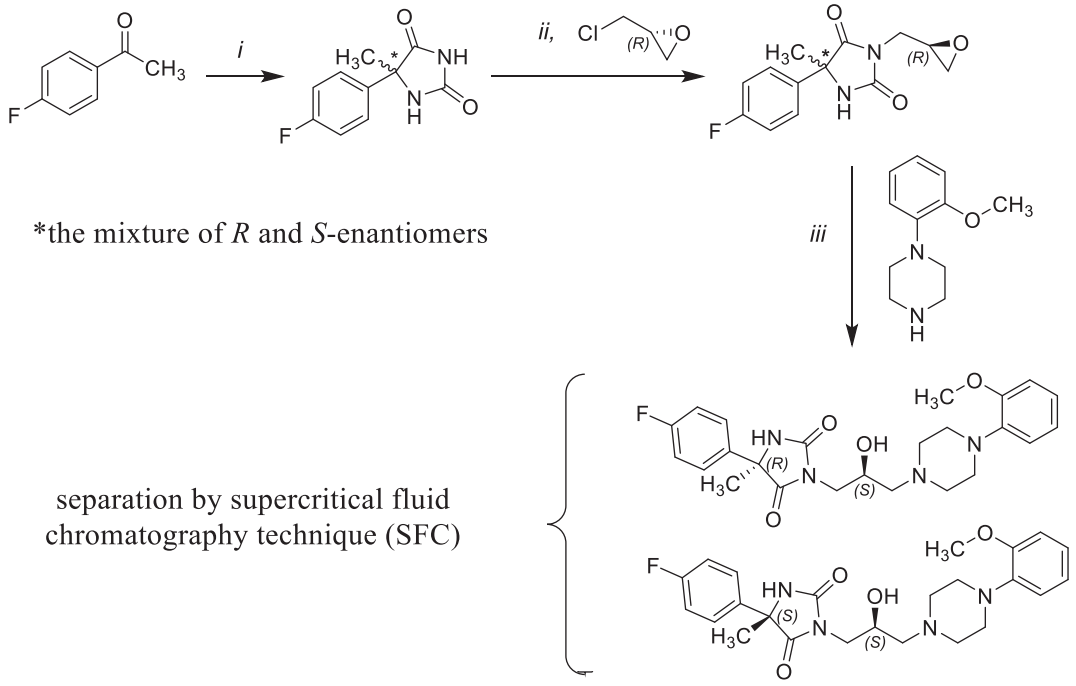

Scheme 1. The synthetic pathway for **MF-8**'s stereoisomers: (*i*) KCN, $NH_4(CO_3)_2$, H_2O/ethanol, 50 °C; yield 54% (*ii*) NaOH, H_2O, rt, yield 61%(*S*)/70%(*R*)**; (*iii*) isopropanol, reflux, yield 45%(*S*)/49%(*R*)**. The analogous approach was applied using *S*-epichlorhydrin to obtain pair of diastereoisomers with configuration *R* of carbon linked with hydroxyl group. *configuration at C5 of hydantoin has not been determined experimentally yet. **configuration of carbon atom bound to hydroxyl group (C7).

Table 1
The enantiopurity for isolated stereoisomers of **MF-8*rac***.

Compound	Structure	Diastereoisomeric excess
MF-8*rac*	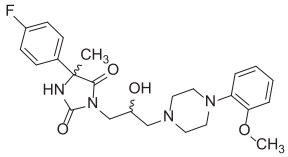	–
MF-8A	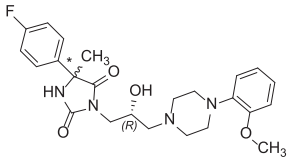	100
MF-8B	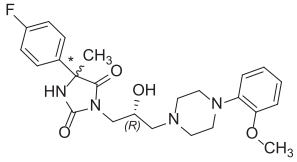	92
MF-8C	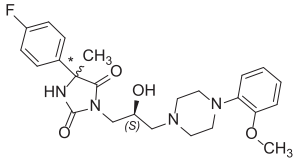	100
MF-8D	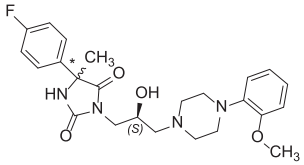	98

Both hydroxy groups, from the **MF-8** molecule and the solvent, are involved in hydrogen bonds with chlorine anion. In the presented crystal structure, it is not observed typical interaction of chlorine anion with protonated nitrogen atom [25], but the oxygen atom of hydroxy group from the solvent interacts with protonated nitrogen atom (N2). The nitrogen atom (N1) of hydantoin moiety is also engaged in hydrogen bond with chlorine anion. Furthermore, the crystal structure is stabilized by C—H···O, C—H···Cl, C—H···F and C—H···π contacts.

2.2.2. *DFT-aided estimation of the absolute configuration for stereoisomers **MF-8A**-**MF-8D***

Configuration at hydroxy-substituted carbon (C7, Fig. 4) was the only one experimental information to base on due to the specific reaction mechanism of the alkylation method used. Thus, it is confirmed that **MF-8A** and **MF-8B** are at C7-*R* configuration, while **MF-8C** and **MF-8D** are at C7-*S*, while, the configuration at C5 was the problem to solve. Although the properties of diastereoisomers in achiral conditions are expected to be different, the ^{1}H NMR spectra for all four stereoisomers (**MF-8A**-**MF-8D**) showed high similarity (see Experimental chapter).

A slight, but relatively the most noticeable, difference could be observed in the case of chemical shifts for proton at hydantoin N1-nitrogen (Table S1, Supplementary) but this fragment is rather far from both stereogenic centers and the difference more probably may refer to a blurred detection related to the nature of the signal (broad singlet). Thus, we tried to focus on the protons in closer surroundings of the stereogenic center C5. In the case of chemical shifts for protons of both, the phenyl (C24, C26, Fig. 4) and the methyl group (C21, Fig. 4), substituted at position C5, a slight decrease was observed if comparing **MF-8A** to **MF-8B** as well as **MF-8C** to **MF-8D**. In this context, computational DFT methods have been applied in term to predict ^{1}H NMR chemical shifts for each stereoisomer of **MF-8** with defined absolute configurations, *i.e.*: (5*R*,7*R*), (5*S*,7*R*) (5*S*,7*R*) and (5*S*,7*S*), respectively. The stereoisomers were built on the basis of crystal structure (Fig. 4) and

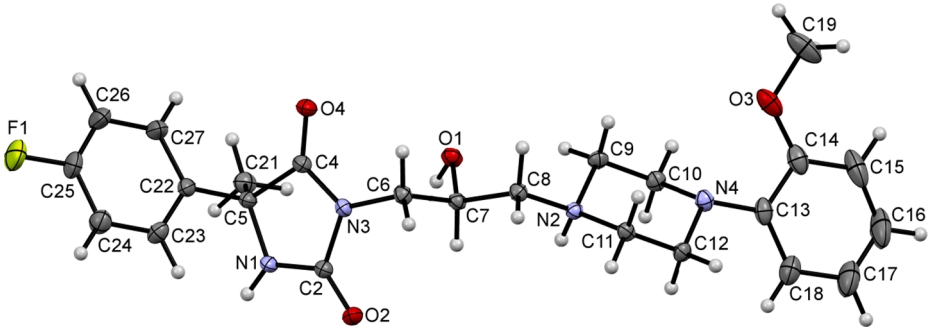

Fig. 4. The molecular structure of **MF-8** showing the atom numbering scheme. Displacement ellipsoids are drawn at the 30% probability level.

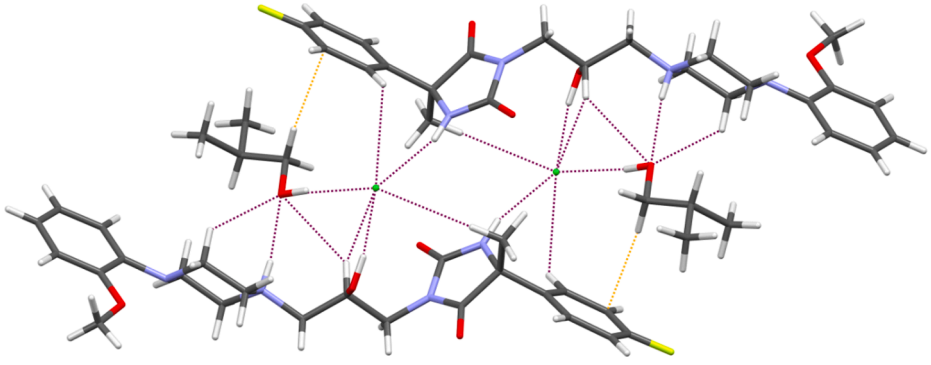

Fig. 5. The interactions of two **MF-8** molecules with chlorine anions and 2-methylpropan-1-ol. For clarity, only carbon atoms with the higher occupancy of the disordered solvent are presented. Purple dashed lines indicate hydrogen bonds, orange C—H···π contacts. (For interpretation of the references to colour in this figure legend, the reader is referred to the web version of this article).

their geometries were optimized on the TPSSh/def2-TZVPP level of theory. The TPSSh functional was selected among six DFT methods, based on test calculations results (see Computational methods section for more details). Then, M06/def2-TZVPP NMR calculations, including solvent effects (DMSO), were performed to determine ^{1}H NMR chemical shifts for the **MF-8** stereoisomers.

In order to decode the most probable configuration, the two-step assumption has been applied, based on the qualitative similarity between calculated and experimental NMR results (Fig. 6, Table S1, Supplementary).

In the first step, the concordance of the order of experimental chemical shifts (δ-values) for the Ph-3,5-H protons of considered stereoisomers (B > A and C > D) with the calculated one [(5*S*,7*R*) > (5*R*,7*R*) and (5*R*,7*S*) > (5*S*,7*S*)] was under consideration (Fig. 6a). In the next step; the similar relationship of the calculated and experimental δ-values for 5-CH_3 protons in pairs of 7R (A,B)- and 7S (C,D)- stereoisomers, respectively, was analyzed (Fig. 6b). Thus, the relationship for 7*R* stereoisomers (A > B) was corresponding to the calculated one, as follows: (5R,7R) > (5S,7R), while that for 7*S*-pair (C > D) corresponded to (5*R*,7*S*)>(5*S*,7*S*). Both assumptions, based on this "semi-empirical" approach, allowed us to assign the stereoisomers configuration in the following order: (5*R*,7*R*) for **MF-8A**, (5*S*,7*R*) for **MF-8B,** (5*R*,7*S*) for **MF-8C** and (5*S*,7*S*) for **MF-8D.** At the absence of any sufficient experimental data, this "sequence" was established as the most probable to use for further consideration within this study and revised by docking simulation in respect to experimental receptor binding results.

2.3. Radioligand binding assays and functional studies

Radioligand binding assays were applied to determine the affinity and selectivity profiles of each of the **MF-8**′s stereoisomers for both, human serotonin 5-HT_{7b}R and 5-HT_{1A}R, which were stably expressed in HEK-293 cells. Interestingly, there are significant differences in 5-HT_7 affinity among the stereoisomers (Table 2), with the most profitable K_i value for stereoisomer **MF-8A** (3 nM) and the least profitable for **MF-8D** (366 nM). All the presented isomers maintained significant selectivity over 5-HT_{1A} receptor.

In order to assess the intrinsic activity of compounds **MF-8A-MF-8D**, the functional assays were performed in which the ability to decrease cAMP level was measured. The results correlate very well with radioligand binding assays with the analogous activity increase in series **MF-8D** < **MF-8B** < **MF-8C** < **MF-8A** with the very strong antagonistic activity of **MF-8A** with K_b = 24 nM, the more profitable than the racemic mixture (K_b = 58 nM).

Table 2
The radioligand binding and functional tests results for **MF-8*rac*** and its stereoisomers.

Compound	$K_i \pm SD$ [nM]		$K_b \pm SD$ [nM]
	5-HT_{1A}	5-HT_7	5-HT_7
MF-8*rac*	121 ± 17	**3** ± 2	**58** ± 12
MF-8A (5*R*, 7*R*)*	832 ± 68	**3** ± 1	**24** ± 7
MF-8B (5*S*, 7*R*)*	1433 ± 219	**44** ± 6	**585** ± 94
MF-8C (5*R*, 7*S*)*	427 ± 34	**26** ± 5	**397** ± 68
MF-8D (5*S*, 7*S*)*	2370 ± 512	**366** ± 53	**99230** ± 33111

*the most probable configuration not confirmed experimentally.

2.4. In vitro ADME-Tox studies

The ADME-Tox parameters of **MF-8**′s stereoisomers were evaluated by *in vitro* methods and compared to **MF-8*rac***. All the applied materials and methods were described in our previous studies [19,23,26,27]. The results obtained for **MF-8*rac*** and stereoisomers **MF-8A**-**MF-8D** were summarized in Table 3.

The bioavailability of **MF-8*rac*** and stereoisomers was evaluated in following assays: parallel artificial membrane permeability assay (PAMPA), Caco-2 cell-based absorption model and by determination of their potential induction or inhibition activity against Pgp - the important efflux pump which is present in both, intestinal epithelium and blood–brain barrier (BBB).

The obtained data from PAMPA were present as permeability coefficient *Pe* calculated according formulas provided by the manufacturer. Two references were used in this study - the antibacterial drug norfloxacin (NFX) with calculated very low $Pe = 0.56 \times 10^{-6}$ cm/s and highly-permeable caffeine (CFN) with *Pe* value estimated to 15.1×10^{-6} cm/s. All examined stereoisomers showed good passive penetration

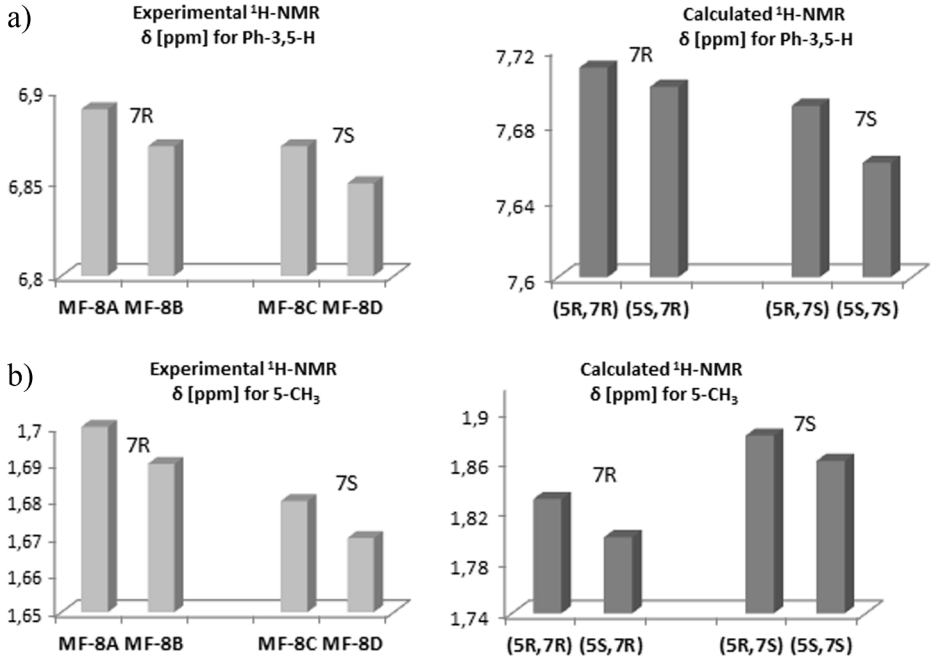

Fig. 6. The qualitative concordance between calculated and experimental chemical shifts (δ) in ^{1}H NMR spectra for the obtained stereoisomers of **MF-8;** a) the comparison for 5-Ph-3,5- protons; b) the comparison for protons of 5-CH_3 group.

Table 3
ADME-Tox parameters of **MF-8*rac*** and stereoisomers.

Parameter	**MF-8*rac***	**MF-8A**	**MF-8B**	**MF-8C**	**MF-8D**
PAMPA (*Pe*) *10^{-6} cm/s ± SD*	6.1 ± 3.2	5.9 ± 0.4	8.0 ± 3.0	4.1 ± 0.8	8.9 ± 0.2
Caco-2 (P_{app}) *10^{-6} cm/s ± SD*	25.6 ± 0.7	16.4 ± 0.04	19.6 ± 0.1	29.9 ± 0.1	17.50 ± 0.01
Pgp activity *% of basal activity ± SD*	121.5 ± 28.1	155.5 ± 14.6	166.1 ± 9.6	112.2 ± 6.7	139.7 ± 4.0
metabolic pathways in mouse	hydroxylation (M1) demethylation (M2) decomposition/ hydroxylation (M3)	hydroxylation (M1)	hydroxylation (M1) demethylation (M2) decomposition/ hydroxylation (M3)	hydroxylation (M1)	hydroxylation (M1)
mouse CL_{int} *mL*/min/*kg*	44.2	40.3	45.4	54.8	35.7
CYP3A4 activity*	75.4 ± 2.2	83.7 ± 5.6	66.6 ± 3.5	80.9 ± 2.7	59.7 ± 1.9
CYP2D6 activity*	98.7 ± 3.4	90.4 ± 0.6	93.0 ± 3.5	95.7 ± 0.5	97.7 ± 4.2
CYP2C9 activity*	165.7 ± 16.1	107.1 ± 0.5	111.3 ± 0.8	302.6 ± 5.4	82.7 ± 1.6
HepG2 viability**	90.6 ± 6.5	89.2 ± 6.4	88.3 ± 7.4	103.1 ± 9.4	95.0 ± 13.7

*% of control ± SD at 10 μM; ** % of control ± SD at 100 μM.

through the biological membranes in compare to the used references, with calculated *Pe* values in range of 4.1–8.9 × 10^{-6} cm/s (Table 3). The lowest ability to membrane diffusion was observed for stereoisomer **MF-8C**, whereas the highest for stereoisomer **MF-8D**. Interestingly, the calculated for **MF-8*rac*** *Pe* value 6.1 × 10^{-6} cm/s was the average of *Pe*'s determined for all four stereoisomers (Table 3).

The influence of **MF-8*rac*** and stereoisomers on Pgp was determined by the luminescence-based Pgp-Glo™ Assay, which measures the ATP consumption by Pgp. The results were compared to the Pgp basal activity, which was calculated as difference in ATP consumption between not treated samples and treated with 100 μM of Pgp inhibitor Na_3VO_4. Verapamil (VL), which stimulates significantly its activity, was used at 200 μM concentration as the Pgp substrate reference. The significant increase in Pgp ATP consumption was determined at the presence of **MF-8A**, **MF-8B** ($p < 0.001$) and **MF-8D** ($p < 0.05$), whereas for **MF-8*rac*** and stereoisomer **MF-8C** no statistically significant stimulation effect was observed (Fig. 7). Thus, all these evidences showed **MF-8A, MF-8B** and **MF-8D** stereoisomers as the substrates of Pgp.

Caco-2, an immortal human colon carcinoma cell line, is the best-known model of *in vitro* permeability assessment which enables to determine both, the passive and active mechanism of absorption. According to the literature [28], the calculated in Caco-2 model permeability coefficient $P_{app} < 2 \times 10^{-6}$ cm/s indicates low permeability, P_{app} from 2 × 10^{-6} to 20 × 10^{-6} cm/s moderate permeability, whereas compounds with $P_{app} > 20 \times 10^{-6}$ cm/s are considered as high permeable. The calculated here permeability coefficient P_{app} values for

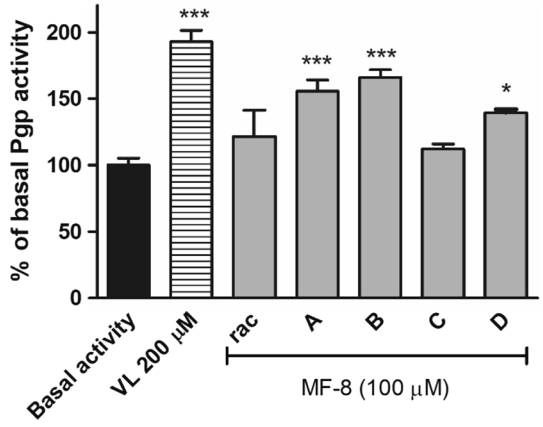

Fig. 7. The effect of Pgp stimulator Verapamil (VL), **MF-8*rac*** and stereoisomers on Pgp basal activity. Statistical significance was evaluated by one-way ANOVA, followed by Bonferroni's comparison test (*$p < 0.05$, ***$p < 0.001$).

MF-8*rac* and stereoisomers were compared to the well-permeable CFN with estimated during this study P_{app} value 22.04 × 10^{-6} cm/s. The obtained results differ between stereoisomers and corelate to the results from Pgp assay. The **MF-8C** stereoisomer which did not show the stimulation effect on Pgp protein activity (Fig. 7) was the highly absorbed compound with calculated $P_{app} = 29.9 \times 10^{-6}$ cm/s. The stereoisomers **MF-8A**, **MF-8B** and **MF-8D**, which significantly stimulated Pgp (Fig. 7), was absorbed in moderate way (P_{app} from 16.4 to 19.6 × 10^{-6} cm/s). Moreover, for **MF-8*rac***, which also did not show the statistically significant increase in Pgp activity (Fig. 7), the high absorption was estimated ($P_{app} = 25.6 \times 10^{-6}$ cm/s). Interestingly, in PAMPA assay lower ability of **MF-8*rac*** to passive transport through the cell membranes was shown in compare to the well-permeable reference CFN, whereas the results from Caco-2 assay showed similar absorption of CFN and **MF-8*rac*** (Table 3). The literature sources indicated only passive mechanism of CFN diffusion through biological membranes. As shown above, some of **MF-8**'s stereoisomers were effluxed by Pgp and despite of this fact, the high absorption of **MF-8*rac*** was still observed. Thus, considering the above, the obtained data indicate the probable uptake transporters activity involvement in **MF-8*rac*** absorption.

The metabolic stability estimation and metabolites identification of **MF-8*rac*** and stereoisomers were performed with use of mouse liver microsomes (MLMs) and UPLC-MS analyses. According to UPLC-MS spectrum of **MF-8*rac*** after 2 h incubation with MLMs, this compound was metabolized mainly into one metabolite M1 with molecular mass $m/z = 473.26$ and into slight amounts of two more metabolites M2 ($m/z = 443.23$) and M3 ($m/z = 342.06$) (Fig. 8). Interestingly, the presence of M2 and M3 was identified only in the reaction mixture with stereoisomer **MF-8B**, whereas **MF-8A**, **MF-8C** and **MF-8D** were metabolized only into M1 (Fig. 8). Thus, only **MF-8B** stereoisomer metabolic pathways were found to be responsible for the presence of M2 and M3 in the **MF-8*rac*** reaction mixture. Moreover, t_R and m/z values of M1 and M2 obtained here by MLMs were similar to the metabolites of **MF-8*rac*** obtained in our previous studies in the presence of human liver microsomes (HLMs) [19].

It shows, that these two metabolic pathways, identified previously as hydroxylation (M1) and demethylation (M2) occurred in both, human and mouse species. The molecular mass of obtained during this study by MLMs additional metabolite M3 ($m/z = 342.06$) corresponds to compound's decomposition followed by double hydroxylation. The most probable structure of M3 metabolite was proposed in Fig. 9.

Next, the intrinsic clearance (CL_{int}) of **MF-8*rac*** and stereoisomers was calculated by measuring of compound's disappearance with time in the presence of MLMs, according to proposed by Obach methods and formulas [28]. The results have shown close for all stereoisomers CL_{int} values in range of 35.7 – 54.8 ml/min/kg (Table 3). Compound **MF-8D**

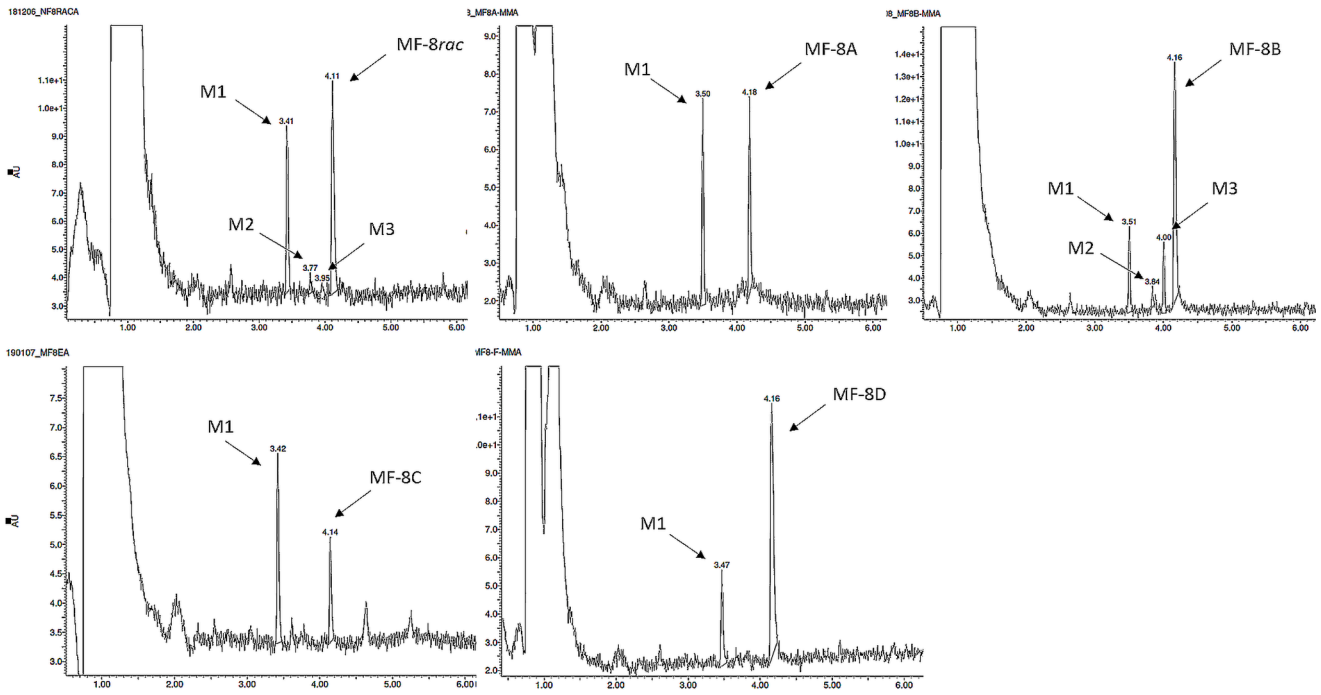

Fig. 8. UPLC spectra of the reaction mixture after 120 min incubation of **MF-8*rac*** and stereoisomers with MLMs.

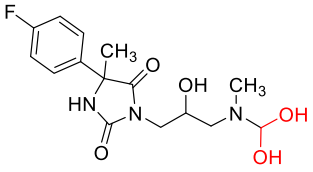

Fig. 9. The most probable structure of metabolite M3 (m/z = 342.06).

with the lowest CL_{int} was determined as the most metabolically stable stereoisomer, whereas the highest CL_{int} was shown for stereoisomer **MF-8C**. The calculated for **MF-8*rac*** CL_{int} = 44.2 ml/min/kg was found as the average of CL_{int} values determined for all four stereoisomers (Table 3). Thus, according to the classification bands for microsomal assays [29], **MF-8C** showed the high clearance (>47.0 ml/min/kg), whereas **MF-8*rac*** and stereoisomers **MF-8A**, **MF-8B** moderate ones as results for these compounds were between 8.6 and 47 ml/min/kg.

The potential DDI predictions were performed with use of P450-Glo™ assays, which enable to measure luminescently the respective CYP isoform activity. The influence of **MF-8*rac*** and stereoisomers on CYP3A4, 2D6 and 2C9 isoforms was examined at the 10 μM concentration each and compared to 1 μM of appropriate strong CYP inhibitor: ketoconazole (KE), quinidine (QD,) and sulfaphenazole (SE), respectively. The statistically significant ($p < 0.001$) CYP3A4 inhibition effect was observed for all tested compounds (Fig. 10a).

However, the inhibitory potential differed between tested compounds. Stereoisomer **MF-8D** showed the highest effect (59.7% of CYP3A4 activity) whereas **MF-8A** the lowest one (83.7% of CYP3A4 activity). **MF-8*rac*** inhibition of CYP3A4 was determined as the resultant of all stereoisomers' inhibition effects (Table 3). No significant effect of **MF-8*rac*** and stereoisomers on CYP2D6 activity was observed (Fig. 10b, Table 3). On the other hand, an interesting effect of tested compounds on CYP2C9 activity was found as stereoisomer **MF-8C** strongly induced its activity up to 302.6% of control activity, stereoisomer **MF-8D** significantly ($p < 0.05$) decreased its activity to 82.7% of control, whereas no changes in the presence of **MF-8A** and **MF-8B** were observed (Fig. 10c, Table 3). Similarly to CYP3A4, the **MF-8*rac*** action on CYP2C9 was estimated as a result of all the stereoisomers effects.

The *hepatoma* HepG2 cell culture was used to determine the hepatotoxicity of **MF-8*rac*** and stereoisomers. As shown in Fig. 11 no statistically significant decrease in cells' viability was observed for all

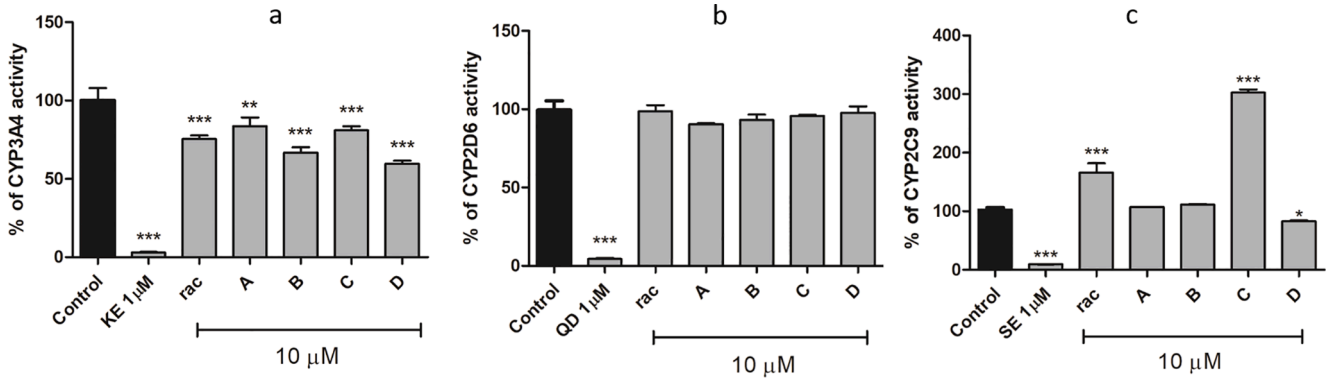

Fig. 10. The effect of the respective inhibitor, **MF-8*rac*** and stereoisomers on CYP3A4 (a), CYP2D6 (b) and CYP2C9 (c) activity. Statistical significance was evaluated by one-way ANOVA, followed by Bonferroni's comparison test (*$p < 0.05$, **$p < 0.01$, ***$p < 0.001$).

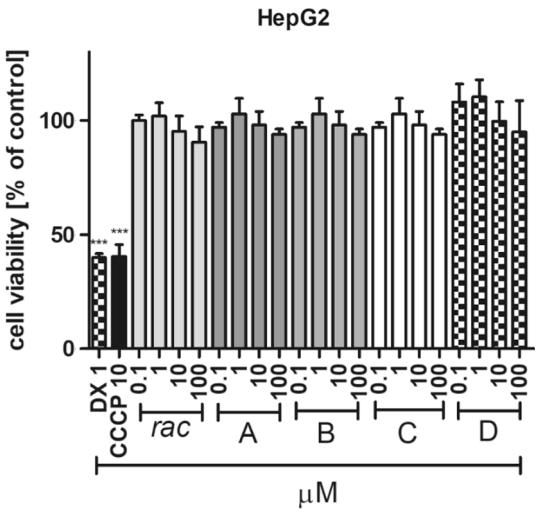

Fig. 11. The effect of **MF-8*rac***, stereoisomers and references: doxorubicin (DX, 1 μM), mitochondrial toxin carbonyl cyanide 3-chlorophenyl-hydrazone (CCCP, 10 μM) on *hepatoma* HepG2 cell line viability. Statistical significance was evaluated by one-way ANOVA, followed by Bonferroni's comparison test (***p < 0.001).

compounds in all used concentrations after 72 h - long incubation.

These results are in accordance with our previous hepatotoxicity examination of **MF-8*rac***, where no significant decrease of the ATP level in HepG2 cells was found, even at the highest used concentration 100 μM [23].

2.5. Docking and MD simulation support for the assays in vitro

In order to insight into the molecular interactions of stereoisomers (**MF-8A**–**MF-8D**) with the target 5-HT$_7$R and CYP2C9 as selected ADME-Tox target docking and molecular dynamic (MD) simulations have been performed. These computer-aided studies were also performed in terms to confirm the configurations found on the basis of a comparison of experimental affinity results to those of simulated using the compounds with defined configurations at C5 and C7, respectively (Fig. 4).

2.5.1. Docking studies and MD simulation to 5-HT$_7$ homology model

All the **MF-8** stereoisomers were docked into 5-HT$_7$R homology models to analyze the differences in protein–ligand interaction. The docking poses and, additionally, interaction matrices of ligand-receptor contacts are presented in Fig. 12.

In general, the most active compound (**MF-8A**), with K_i values towards 5-HT$_7$R of 3 nM adopted significantly different docking poses in comparison to other stereoisomers tested. It is located deepest in the binding site, although, similarly to **MF-8B**, **MF-8C**, and **MF-8D**, it still formed interactions with amino acids from the second extracellular loop (ECL2). **MF-8A** also interacted with the highest number of amino acids from the third transmembrane helix (TM3), the lowest number of amino acids from the 7th transmembrane helix (TM7) and did not interact with F 6x52. All of the compounds formed charged assisted hydrogen bond with D3.32 residue and possessed aromatic pi-pi stacking interactions with F6.51. **MF-8C**, that was also quite active towards 5-HT$_7$R (K_i = 26 nM), interacted only with one amino acid from the ECL2, while with more amino acids from the TM7 and demonstrated different orientation of the methoxyl group, as main differences in docking poses in comparison to the remaining compounds. Interestingly, although **MF-8B** and **MF-8D** displayed significantly different affinity towards 5-HT$_7$R (K_i = 44 nM and 366 nM, respectively), they adopted similar docking poses with fluorine atoms pointing towards the ECL2.

As docking results do not fully explained observed relationships between compound structure and activity, MD simulations were carried

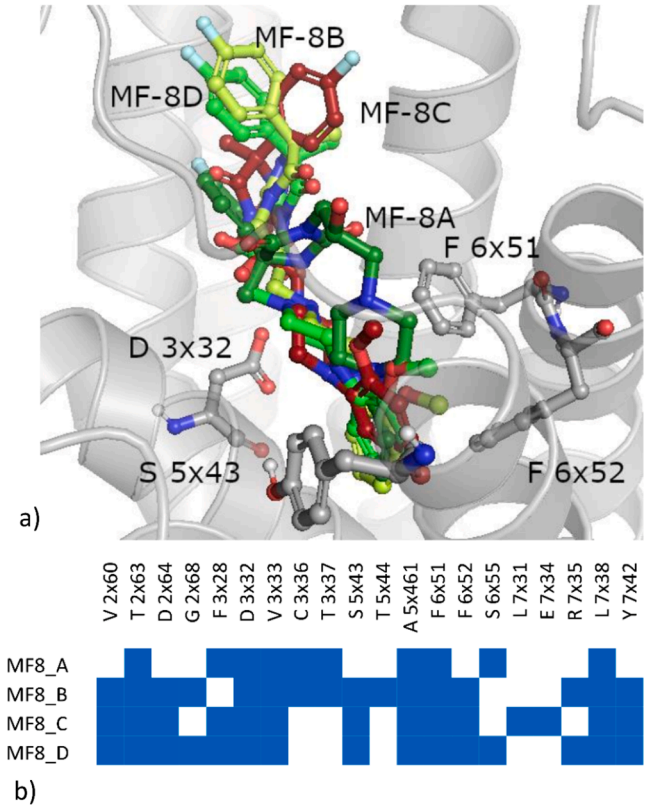

Fig. 12. a) Docking of **MF-8** stereoisomers to 5-HT$_7$R homology model; b) ligand–protein contacts occurring in the obtained complexes.

out. The changes of the set of interacting amino acids for each of the considered diastereoisomers in time occurring during MD simulation studies are presented in Supplementary Information (Fig. S11).

The comparison of the obtained results indicates that all of the stereoisomers of **MF-8** formed a strong, and conserved during the whole simulation, interaction with D3.32 (ASP93). This interaction has been indicated as crucial for 5-HT$_7$R activity by many previous studies [30]. For stereoisomer **MF-8D**, it is also characteristic the relatively strong interaction with CLI residues from the ELC2 (CYS162, LEU163, ILE164) that was also not lost during the whole simulation time. The most active **MF-8A** formed statistically the strongest interaction with E 7x34 (GLU 257), S 6x55 (SER 238) and F 3x28 (PHE 89).

2.5.2. Docking studies and MD simulation to CYP2C9

Further molecular modeling studies (docking and MD simulations) were performed in order to explain the observed dependencies between configuration of particular **MF-8** stereoisomers and their influence on CYP2C9 activity (Fig. 10c). As a reference, a set of CYP2C9 substrates from the ChEMBL database [31] were also docked to the respective protein. They were selected on the basis of the following criteria: description of activity by AC50 parameter and the reported AC50 value below 100 nM. The docking poses obtained for particular **MF-8** stereoisomers are presented in Fig. 13.

The main differences in docking poses that are observed between **MF-8D** (depicted in green, compound inducing the CYP2C9 activity to the least extent) and other forms of **MF-8** (depicted in orange, cyan and magenta for **MF-8A**, **MF-8B**, and **MF-8C**, respectively) are connected with bend conformation of **MF-8D**, although the set of amino acids interacting with particular compounds examined is similar. However, the position of aromatic rings is significantly different for **MF-8D** in comparison to other stereoisomers. The more detailed analysis of docking results is provided by ligand interaction diagrams presented in the Supporting Information (Fig. S12). On the other hand, **MF-8C**, the

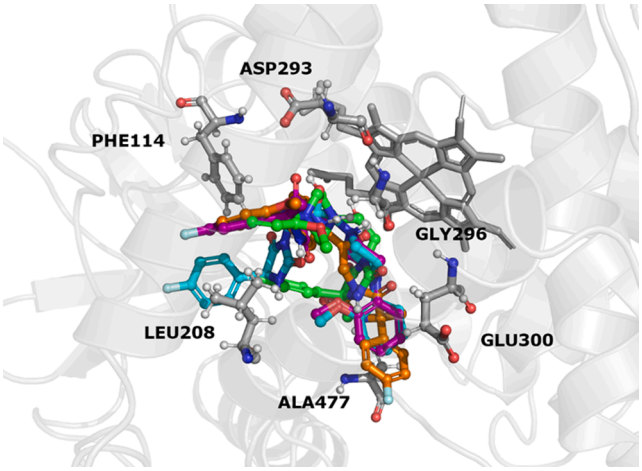

Fig. 13. Docking poses obtained for examined compounds to CYP2C9 – **MF-8A**: orange, **MF-8B**: cyan, **MF-8C**: magenta, and **MF-8D**: green. (For interpretation of the references to colour in this figure legend, the reader is referred to the web version of this article).

least stable compound in terms of CYP2C9-mediated metabolism adopted similar docking pose to **MF-8A** that was three times more stable than **MF-8C**; therefore, analogously to analysis of compounds activity towards 5-HT_7R, MD simulations were carried out (Fig. S13).

Comparing results of MD simulations, especially for **MF-8A** and **MF-8C** that adopted similar docking pose, but displayed significantly different influence on CYP2C9 activity, revealed change in the orientation in the binding site for the former compound, resulting in making contacts with PHE100, LEU102, ALA103, ARG108, and ALA297, which was not observed for more stable **MF-8A**.

3. Conclusions

Within this comprehensive study, the all four stereoisomers of previously described, highly potent 5-HT_7R ligand with antidepressant activity on mice (**MF-8**), were isolated and biologically evaluated in terms of pharmacodynamic and pharmacokinetic profile. As the configuration for one of two present chiral centers was not possible to be determined experimentally, DFT calculations of ^{1}H NMR chemical shifts for optimized stereoisomers geometries, based on the crystal structure of **MF-8**, have been applied to perform appropriate predictions, while docking and dynamic simulations in comparison to experimental screening results, were used to confirm that prediction. The obtained experimental data for respective stereoisomers (**MF-8A-MF-8D**) have indicated the significant influence of stereochemistry on either the 5-HT_7R activity or ADME-Tox properties *in vitro*. The affinity for 5-HT_7R differed in the range of 3–366 nM of K_i values, with respect to configurations at both, hydantoin position C5 or linker position C7. The docking studies showed significantly deeper location of **MF-8A** (5R, 7R), the most potent stereoisomer ($K_i = 3$ nM), in the 5-HT_7R binding site in comparison to other stereoisomers, thus elucidating its high affinity and confirming the predicted configuration. The obtained results has also confirmed stereochemistry-dependent influence of the tested compounds set on P-glycoprotein efflux, absorption in Caco-2 model, metabolic pathway, CYP3A4 and CYP2C9 activity, thus pharmacokinetic profile of racemate is the combination of properties coming from particular stereoisomers. The comprehensive results of ADME-Tox and radioligand binding assays *in vitro* studies have demonstrated the best profile for the stereoisomer **MF-8A** with estimated configuration of (5R, 7R).

Although the DFT–aided simulation performed seems to correlate well with the docking results in terms of assignment of absolute configurations of chiral center at hydantoin (C5), further experimental determination of the proposed configuration is needed to fully confirm the presented data. In the light of all the herein described results and the fact that the racemic **MF-8** showed significant antidepressant effects in mice, the corresponding pharmacological assays *in vivo* for particular stereoisomers (**MF-8A**) would be purposeful in the close future.

4. Experimental

4.1. Chemical synthesis

^{1}H NMR and ^{13}C NMR spectra were recorded on a Varian Mercury VX 300 MHz PFG instrument (Varian Inc., Palo Alto, CA, USA) in DMSO-d_6 at ambient temperature using the solvent signal as an internal standard. Data are reported using following abbreviations: s, singlet; bs, broad singlet; d, doublet; t, triplet; def, deformated; Ph, phenyl; Pp, piperazine; Ar, aromatic. Thin-layer chromatography (TLC) was performed on precoated Merck silica gel 60 F254 aluminium sheets, and the solvent system used was methylene chloride (DCM)/methanol (MeOH) 95:5. The mass of compounds were recorded on a Waters ACQUITY^{TM} UPLC (Waters, Milford, MA, USA) coupled to a Waters TQD mass spectrometer (electrospray ionization mode, EDI-tandem quadrupole). Retention times (t_R) are given in minutes. The UPLC/MS purity of all final compounds were determined (%). The reaction conditions for Bucherer-Berg's condensation and *N*-alkylation were applied according to already described procedure [20,21]. Physicochemical data for both oxiranes are presented in Supplementary Information.

4.1.1. General procedure for condensation of oxiran with 1-(2-methoxyphenyl)piperazine

The starting materials: 5-(4-fluorophenyl)-5-methyl-3-(((*S*)oxiran-2-yl)methyl)imidazolidine-2,4-dione (3.5 mmol) and 1-(2-methoxyphenyl)piperazine (3.0 mmol) were dissolved in isopropanol in round-bottom flask and refluxed for 30 min. The reaction progress was monitored with TLC (DCM/MeOH 95:5). After the completion of reaction, the mixture was concentrated under reduced pressure. The crude product was dissolved in DCM and washed with water and brine. The organic phase was dried oved Na_2SO_4, filtered and concentrated under reduced pressure. The analogous procedure were applied using 5-(4-fluorophenyl)-5-methyl-3-(((*R*)oxiran-2-yl)methyl)imidazolidine-2,4-dione as starting material.

The resulted two pairs of diastereoisomers were separated using supercritical fluid chromatography (SFC) technique at Jagiellonian Center of Innovation. The particular parameters for analytical and preparative conditions are presented in Table 4. The appropriate spectral analyses are included in Supplementary information. For both SFC separations 100 mg of samples were used resulting with 16 mg of **MF8-A**, 12 mg of **MF8-B**, 7 mg of **MF8-C** and 13 mg of **MF8-D**.

4.1.1.1. (R)-5-(4-fluorophenyl)-3-((R)-2-hydroxy-3-(4-(2-methoxyphenyl)piperazin-1-yl)propyl)-5-methylimidazolidine-2,4-dione ***(MF-8A)***. White solid. LC/MS±: purity 100%, t_R 4.18 (ESI) *m/z* $[M + H]^+$ 457.24. ^{1}H NMR δ (ppm): 1.70 (s, 3H, 5-CH_3), 2.28–2.50 (m, 2H, Pp-CH_2), 2.92–3.08 (m, 8H, Pp-H), 3.41 (br. s, 2H, N3-CH_2), 3.78 (s, 3H, OCH_3), 3.90–4.20 (m, 1H, C*H*OH), 4.85 (br. s, 1H, CHO*H*), 6.89 (s, 2H, 5-Ph-3,5-H), 6.95 (s, 2H, 5-Ph-2,6-H), 7.20–7.26 (t def., 2H, PpPh-4,6-H), 7.53–7.57 (m, 2H, PpPh-3,5-H), 8.96 (br.s, 1H, N1-H)

4.1.1.2. (S)-5-(4-fluorophenyl)-3-((R)-2-hydroxy-3-(4-(2-methoxyphenyl)piperazin-1-yl)propyl)-5-methylimidazolidine-2,4-dione ***(MF-8B)***. White solid. LC/MS±: purity 98.94%, t_R 4.15 (ESI) *m/z* $[M + H]^+$ 457.24. ^{1}H NMR δ (ppm): 1.69 (s, 3H, 5-CH_3), 2.28 (t def., 2H, Pp-CH_2), 2.50 (br. s, 4H, Pp-2,6-H), 2.91 (br. s, 4H, Pp-3,5-H), 3.40 (br. s, 2H, N3-CH_2), 3.77 (s, 3H, OCH_3), 3.91 (br. s, 1H, C*H*OH), 4.86 (br. s, 1H, CHO*H*), 6.87 (s, 2H, 5-Ph-3,5-H), 6.93 (s, 2H, 5-Ph-2,6-H), 7.20–7.23 (t def., 2H, PpPh-4,6-H), 7.54–7.58 (m, 2H, PpPh-3,5-H), 8.90 (br. s, 1H, N1-H).

Table 4
The parameters for analytical and preparative separation of both pairs of **MF-8**′s diastereoisomers (**MF-8A-B** and **MF-8C-D**).

Parameter		Analytical method		Preparative method	
Equipment and software		Acquity UPC2 Waters, PDA Detector Type HPLC 2998 800 nm, Empower 3 Software Build 3471 SPs		Fully automated preparative SFC system connected with PDA detector (2998 Waters) and Mass detector (Acquity QDa). MassLynx Software V.4.1	
Column		Diacel Chiralpac IC 3 um 3.0 × 150 mm		Diacel Chiralpac IC 5 um 20.0 × 250 mm	
Pressure ABPR		2000 psi		120 bar	
Oven temperature		38 °C		38 °C	
Wavelength		254 nM; 3D scan		254 nM; 3D scan	
Solvent B		MeOH + 0,5% TEA		MeOH + 0,5% TEA	
		Diastereoisomers MF-8A-B	**Diastereoisomers MF-8C-D**	**Diastereoisomers MF-8A-B**	**Diastereoisomers MF-8C-D**
Time		20 min	15 min	20 min	15 min
Flow rate		1.5 ml/min	1.5 ml/min	100 ml/min	100 ml/min
Mobile phase	**% CO_2**	85	85	85	85
	%B	15	15	15	15

4.1.1.3. (R)-5-(4-fluorophenyl)-3-((S)-2-hydroxy-3-(4-(2-methoxyphenyl)piperazin-1-yl)propyl)-5-methylimidazolidine-2,4-dione ***(MF-8C)***. White solid. LC/MS±: purity 100%, t_R 4.17 (ESI) *m/z* $[M + H]^+$ 457.24. ^{1}H NMR δ (ppm): 1.68 (s, 3H, 5-CH_3), 2.33–2.40 (m, 2H, Pp-CH_2), 2.91–3.09 (m, 8H, Pp-H), 3.40 (br. s, 2H, N3-CH_2), 3.77 (s, 3H, OCH_3), 3.92 (br.s, 1H, C*H*OH), 4.87 (br. s, 1H, CHO*H*), 6.87 (s, 2H, 5-Ph-3,5-H), 6.93 (s, 2H, 5-Ph-2,6-H), 7.21–7.26 (m, 2 h, PpPh-4,6-H), 7.52–7.56 (m, 2H, PpPh-3,5-H), 8.92 (br.s, 1H, N1-H).

4.1.1.4. (S)-5-(4-fluorophenyl)-3-((S)-2-hydroxy-3-(4-(2-methoxyphenyl)piperazin-1-yl)propyl)-5-methylimidazolidine-2,4-dione ***(MF-8D)***. White solid. LC/MS±: purity 97.82%, t_R 4.18 (ESI) *m/z* $[M + H]^+$ 457.17. ^{1}H NMR δ (ppm): 1.67 (s, 3H, 5-CH_3), 2.31–2.32 (d def., 2H, Pp-CH_2), 2.89–3.20 (m, 8H, Pp-H), 3.38–3.40 (t def., 2H, N3-CH_2), 3.77 (s, 3H, OCH_3), 3.90–3.96 (qu def., 1H, C*H*OH), 4.84–4.85 (d def., 1H, CHO*H*), 6.85 (s, 2H, 5-Ph-3,5-H), 6.92 (s, 2H, 5-Ph-2,6-H), 7.20–7.24 (t def., 2 h, PpPh-4,6-H), 7.52–7.56 (m, 2H, PpPh-3,5-H), 8.90 (br.s, 1H, N1-H).

4.2. Receptors studies in vitro

4.2.1. Affinities for human 5-HT_{1A} and 5-HT_{7b} receptors

HEK-293 cells with stable expression of human 5-HT_{1A}, 5-HT_{7b} receptors (prepared with the use of Lipofectamine 2000) were maintained at 37 °C in a humidified atmosphere with 5% CO_2 and grown in Dulbecco's Modifier Eagle Medium containing 10% dialyzed fetal bovine serum and 500 μg/ml G418 sulfate. For membrane preparation, cells were subcultured in 150 cm^2 flasks, grown to 90% confluence, washed twice with phosphate buffered saline (PBS) prewarmed to 37 °C and pelleted by centrifugation (200 g) in PBS containing 0.1 mM EDTA and 1 mM dithiothreitol. Prior to membrane preparation, pellets were stored at −80 °C. Cell pellets were thawed and homogenized in 10 volumes of assay buffer using an Ultra Turrax tissue homogenizer and centrifuged twice at 35,000 × g for 15 min at 4 °C, with incubation for 15 min at 37 °C in-between. The composition of the assay buffers was as follows: for 5-HT_{1A}R: 50 mM Tris HCl, 0.1 mM EDTA, 4 mM $MgCl_2$, 10 μM pargyline and 0.1% ascorbate and for 5- HT_{7b}R: 50 mM Tris HCl, 4 mM $MgCl_2$, 10 μM pargyline and 0.1% ascorbate. All the assays were incubated in a total volume of 200 μl in 96-well microtiter plates for 1 h at 37 °C, except those for 5-HT_{1A}R which were incubated at room temperature. The process of equilibration was terminated by rapid filtration through Unifilter plates with a FilterMate Unifilter 96 Harvester (PerkinElmer, USA). The radioactivity bound to the filters was quantified on a Microbeta TopCount instrument (PerkinElmer, USA). For competitive inhibition studies, the assay samples contained the following as radioligands (PerkinElmer, USA): 2.5 nM [^{3}H]-8-OH-DPAT (135.2 Ci/ mmol) for 5-HT_{1A}R; 0.8 nM [^{3}H]-5-CT (39.2 Ci/mmol) for 5-HT_7R or 2.5 nM [^{3}H]-raclopride (76.0 Ci/mmol) for D_{2L}R. Non–specific binding was defined with 10 μM of 5-HT in 5-HT_{1A}R and 5-HT_7R binding experiments. Each compound was tested in triplicate at 7 concentrations (10^{-10}–10^{-4} M). The inhibition constants (K_i) were calculated from the Cheng-Prusoff equation [32]. For all the binding assays, results were expressed as means of at least two separate experiments (SD ≤ 19%).

4.2.2. Functional assays

The functional properties of compounds **MF-8*rac*** and **MF-8A-MF-8D** on 5-HT_{7b}R were evaluated using their ability to inhibit cAMP production induced by 5-CT (10 nM) – a 5-HT_{7b}R agonist, in HEK-293 cells overexpressing 5–HT_{7b}R. Each compound was tested in triplicate at 8 concentrations (10^{-11} – 10^{-4} M).

Cells (prepared with the use of Lipofectamine 2000) were maintained at 37 °C in a humidified atmosphere with 5% CO_2 and were grown in Dulbeco's Modifier Eagle Medium containing 10% dialysed foetal bovine serum and 500 μg/ml G418 sulphate. For functional experiments, cells were subcultured in 25 cm flasks, grown to 90% confluence, washed twice with prewarmed to 37 °C phosphate buffered saline (PBS) and were centrifuged for 5 min (160 × g). The supernatant was aspirated, the cell pellet was resuspended in stimulation buffer (1 × HBSS, 5 mM HEPES, 0.5 mM IBMX, 0.1% BSA). Total cAMP was measured using the LANCE cAMP detection kit (PerkinElmer), according to the producer's directions. For cAMP levels quantification, cells (5 μl) were incubated with compounds (5 μl) for 30 min at room temperature in 384-well white opaque microtiter plate. After incubation, the reaction was stopped and cells were lysed by the addition of 10 μl working solution (5 μl Eu-cAMP and 5 μl ULight-anti-cAMP). The assay plate was incubated for 1 h at room temperature. Time-resolved fluorescence resonance energy transfer (TR-FRET) was detected by an Infinite M1000 Pro (Tecan) using instrument settings from LANCE cAMP detection kit manual.

4.3. Crystallographic studies

Single crystals suitable for an X-ray analysis were obtained from 2-methylpropan-1-ol by slow evaporation of the solvent at room temperature.

The intensity data for single crystal were collected using the Oxford Diffraction SuperNova four circle diffractometer, equipped with the Mo (0.71069 Å) Kα radiation source and graphite monochromator. The phase problem was solved by direct methods using SIR-2014 [33] and all non-hydrogen atoms were refined anisotropically using weighted full-matrix least-squares on F^2. Refinement and further calculations were carried out using SHELXL [34]. The hydrogen atoms bonded to carbon atoms were included in the structure at idealized positions and were refined using a riding model with U_{iso}(H) fixed at 1.2 U_{eq} of C with the exception of hydrogen atoms in methyl group for which U_{iso}(H) fixed at 1.5 U_{eq}. Hydrogen atoms attached to nitrogen and oxygen atoms were found from the difference Fourier map and refined without any restraints. The molecule of 2-methylpropan-1-ol is disordered. The occupancy factors of the carbon atoms were refined to be 0.62 and 0.38 for the major and minor components, respectively. For molecular graphics MERCURY [35] program was used.

$C_{24}H_{31}FN_4O_4^{+}Cl^{-}\cdot C_4H_9OH$, $M_r = 567.09$, crystal size = 1.17 × 0.76 × 0.07 mm^3, monoclinic, space group $P2_1/c$, a = 17.1443(3) Å, b = 18.8374(3) Å, c = 9.2142(2) Å, V = 2937.2(4) $Å^3$, Z = 4, T = 130(2)K, 40,226 reflections collected, 7109 unique reflections (R_{int} = 0.0390), R1 = 0.0537, w*R*2 = 0.1348 [I > 2σ(I)], R1 = 0.0728, w*R*2 = 0.1503 [all data].

CCDC 1958223 contains the supplementary crystallographic data. These data can be obtained free of charge from The Cambridge Crystallographic Data Centre *via* www.ccdc.cam.ac.uk/data_request/cif.

4.4. DFT calculations methodology

Geometries of the **MF-8** stereoisomers were optimized with the hybrid *meta*-GGA TPSSh [36] functional combined with the triple-ζ valence def2-TZVPP basis set [37]. The starting structure of the (5R,7R) stereoisomer (basic form) was prepared from the crystallographic data for the cationic form of the (5R,7R) **MF-8**. By respective modification, the starting structures of other stereoisomers were built. The TPSSh functional was selected on the basis of test calculations, where the accuracy of six DFT methods in predicting geometry of the basic form of previously obtained similar compound **KKB-4 (**CCDC 1831620) [21] was examined. The obtained mean unsigned errors (MUE) in bond lengths, referred do the experimental crystal structure, were 0.0077, 0.0080, 0.0093, 0.0088, 0.0076 and 0.0083 Å for the B3LYP, B3PW91 [38], LC-ωPBE [39], PBE0 [40], TPSSh and ωB97X-D [41] functionals, respectively. Harmonic vibrational frequencies were calculated for each structure to confirm the potential energy minimum.

Based on the previous works [42–44], the hybrid *meta*-GGA M06 functional [45] and the def2-TZVPP basis set were chosen to calculate absolute ^{1}H shielding constants for the (5R,7R), (5R,7S), (5S,7R) and (5S,7S) stereoisomers of **MF-8** using the GIAO method [46,47]. Solvent effects (DMSO) were included by applying the polarizable continuum model (PCM) [48]. The chemical shifts were calculated using ^{1}H shielding constants for DMSO as the reference (assuming the ^{1}H NMR shift of 2.50 ppm, according to the experimental procedure) computed at the same level of theory. All DFT calculations were performed using the Gaussian 16 software [49].

4.5. Docking and MD simulations

The three-dimensional conformations of compounds and respective protonation states (for pH 7.4 +/- 0.0) were generated with the use of LigPrep [50]. The docking was carried out in Glide [51] in extra precision mode. MD simulations (using Schrodinger's Desmond software [52]) were carried out for each of the obtained ligand-receptor complexes (duration time = 100 ns for 5-HT_7R and 200 ns for simulations with CYP2C9; TIP3P [53] as solvent model and POPC (palmitoyl-oleil-phosphatidylcoline) as membrane model used for 5-HT_7R). The interactions between ligands and the respective protein occurring during whole simulations were analyzed using Simulation Interaction Diagram from the Schrodinger Suite.

4.6. In vitro ADME-Tox studies

The ADME-Tox studies excluding Caco-2 absorption tests were carried out as described previously [19,23,26,27].

4.6.1. References

The following references used in ADME-Tox assays: caffeine (CFN), carbonyl cyanide 3-chlorophenylhydrazone (CCCP), doxorubicin (DX), ketoconazole (KE), nonyl-4-hydroxyquinoline-*N*-oxide (NQNO), norfloxacin (NFX), quinidine (QD) and sulfaphenazole (SE) were purchased from Sigma-Aldrich (St. Louis, MO, USA). Verapamil (VL) and Na_3VO_4 used in Pgp activity studies were provided by Promega (Madison, WI, USA).

4.6.1.1. Caco-2 absorption assay. Caco-2 (ATCC® HTB-37™) cell line was purchased from American Type Culture Collection (Manassas, VG, USA). The cells were cultivated in Dulbecco's Modified Eagle s Medium (DMEM) supplemented with 10% fetal bovine serum (FBS) in a humidified atmosphere of 5% CO_2. The medium was changed every two days and the cells were subcultured at 70–80% confluence. The Corning® 3413 Transwell® 6.5 mm polycarbonate membrane inserts with 0.4 μm pore were purchased from Sigma-Aldrich (Saint Louis, MO, USA). The inserts were pretreated first with 50 μl of the medium for two minutes. Next, the 200 μl of cells were seeded at 2×10^{-4} concentration per insert in apical compartment, whereas 600 μl was added to the basolateral one. The plate was incubated at 37 °C for 14 h and the non-adherent cells were removed. TEER (Transepithelial Electrical Resistance) measurements was started from 18-day after seeding by Millicell ERS-2 Volt-Ohm Meter (Merck Millipore, Burlington, MA, USA). The proper monolayer integrity was determined at 20-day after seeding. Then, the monolayer was rinsed with HBSS and the tested compounds as well as highly permeable reference caffeine was added at 10 μM concentration in HBSS into the apical chambers. The 600 μl of HBSS was added to the basolateral compartments. Lucifer yellow (5 μM) was also added to the apical chambers as the membrane integrity marker. The plate was placed in the orbital shaker (60 rpm) for 2 h at 37 °C. The compounds' concentrations in apical and basolateral wells were analyzed using LC-MS method with internal standard (IS). To confirm the membrane integrity the fluorescence was measured in basolateral compartment by EnSpire multiplate reader (Perkin Elmer, Waltham, MA, USA).

The permeability P_{app} were calculated according to the following formula [54]:

$$P_{app} = dc/dt^*V/(A^*C_0)$$

dc/dt- the change in concentration in the receiving compartment overtime

V- volume of the solution in the receiving compartment (mL)

A- surface area of the membrane (cm^2)

C_0- the initial concentration in the donor compartment (μM)

4.6.1.2. PAMPA. Pre-coated PAMPA Plate System Gentest™ purchased from Corning (Tewksbury, MA, USA) was used for permeability evaluation. The tested compounds and references solutions were prepared in PBS buffer (pH = 7.4) and added to the donor wells (200 μM, 300 μl/well). PBS (200 μl/well) was added to the acceptor wells. All compounds were incubated in triplicate at room temperature for 5 h. Then, the 50 μl was aspirated from each well and diluted next with 50 μl solution of IS. The compounds concentrations in both acceptor and donor wells were estimated by the UPLC-MS analyses, which were performed by UPLC/MS Waters ACQUITY™ TQD system with the TQ Detector (Waters, Milford, USA). The permeability coefficients (*Pe,* cm/s) were calculated according described previously formulas [55].

4.6.1.3. Pgp assay. The luminescent Pgp-Glo™ Assay System was purchased from Promega (Madison, WI, USA). The assay was performed in triplicate according to the protocol provided by manufacturer. **MF-8*rac*** and stereoisomers (100 μM) were incubated with Pgp membranes for 40 min at 37 °C. The luminescence signal was measured by microplate reader EnSpire PerkinElmer (Waltham, MA, USA).

4.6.1.4. Metabolic stability. The intrinsic clearance (CL_{int}) of **MF-8*rac*** and stereoisomers were estimated by incubation with mouse liver microsomes (MLMs) purchased from Sigma-Aldrich (St. Louis, MO, USA). The disappearance of compounds (50 μM) in the presence of MLMs (1 mg/ml) was determined at 5, 15, 30 and 45 min of incubation in 10 mM Tris–HCl buffer (37 °C). The UPLC/MS Waters ACQUITY™ TQD system with the TQ Detector (Waters, Milford, USA) analysis with use of IS allowed for determination of tested compound elimination. The $t_{1/2}$

values and CL_{int} were calculated by protocols and formulas proposed by Obach [29].

The metabolic pathways evaluation of **MF-8*rac*** and stereoisomers was performed by prolonged, 120 min incubation with MLMs. The concentration of compounds, the ingredients of the reaction mixture and UPLC/MS analyses conditions were similar to the described above.

4.6.1.5. Drug-drug interaction prediction. The luminescent CYP3A4, CYP2D6 and CYP2C9 P450-Glo™ assays were purchased from Promega® (Madison, WI, USA). The assays were conducted according to manufacturer recommendations. The compounds were tested in triplicate at the final concentration of 10 μM. The luminescent signal was measured by using a microplate reader EnSpire PerkinElmer (Waltham, MA, USA).

4.6.1.6. Hepatotoxicity. Hepatoma HepG2 (ATCC® HB-8065™) cells were growth in Modified Eagle s Medium (MEM) supplemented with 10% fetal bovine serum (FBS) in a humidified atmosphere of 5% CO_2. For hepatotoxicity evaluation **MF-8*rac*** and stereoisomers were incubated at 96-wells plate with cells for 72 h in the final concentration range (0.1–100 μM). The reference toxin CCCP and DX were added at 10 μM and 1 μM, respectively. The cells' viability was determined by CellTiter 96® AQueous Non-Radioactive Cell Proliferation Assay (MTS) purchased from Promega (Madison, WI, USA). The absorbance was measured using a microplate reader EnSpire (PerkinElmer, Waltham, MA USA) at 490 nm.

Declaration of Competing Interest

The authors declare that they have no known competing financial interests or personal relationships that could have appeared to influence the work reported in this paper.

Acknowledgements

This study was financially supported by Polish National Science Centre (NCN) grant No UMO-2014/15/N/NZ7/03072. SP was supported by the Foundation for Polish Science (FNP) within the START scholarship and by Polish Statutory Research Project N42/DBS/000027.

Appendix A. Supplementary material

Supplementary data to this article can be found online at https://doi.org/10.1016/j.bioorg.2020.104466.

References

[1] M. Ruat, E. Traiffort, R. Leurs, J. Tardivel-Lacombe, J. Diaz, J.M. Arrang, J. C. Schwartz, Molecular cloning, characterization, and localization of a high-affinity serotonin receptor (5-HT7) activating cAMP formation. Proc. Natl. Acad. Sci. 90 (18) (1993) 8547–8551.

[2] J.A. Bard, J. Zgombick, N. Adham, P. Vaysse, T.A. Branchek, R.L. Weinshank, Cloning of a novel human serotonin receptor (5-HT7) positively linked to adenylate cyclase, J. Biol. Chem. 268 (1993) 23422–23426.

[3] T.W. Lovenberg, B.M. Baron, L. de Lecea, J.D. Miller, R.A. Prosser, M.A. Rea, P. E. Foye, M. Racke, A.L. Slone, B.W. Siegel, P.E. Danielson, J.G. Sutcliffe, M. G. Erlander, A novel adenylyl cyclase-activating serotonin receptor (5-HT7) implicated in the regulation of mammalian circadian rhythms, Neuron 11 (3) (1993) 449–458.

[4] K.M. Blattner, D.J. Canney, D.A. Pippin, B.E. Blass, Pharmacology and Therapeutic Potential of the 5-HT 7 Receptor, ACS Chem. Neurosci. 10 (1) (2019) 89–119.

[5] A. Wesołowska, A. Nikiforuk, K. Stachowicz, Potential anxiolytic and antidepressant effects of the selective 5-HT7 receptor antagonist SB 269970 after intrahippocampal administration to rats, Eur. J. Pharmacol. 553 (1-3) (2006) 185–190.

[6] L. Janssen Research & Development, Testing the Ability of JNJ-18038683 to Improve Cognition and Reduce Depressive Symptoms in Stable Bipolar Patients, (n. d.). https://clinicaltrials.gov/ct2/show/study/NCT02466685?term=JNJ-18038683.

[7] P. Bonaventure, C. Dugovic, M. Kramer, P. De Boer, J. Singh, S. Wilson, K. Bertelsen, J. Di, J. Shelton, L. Aluisio, L. Dvorak, I. Fraser, B. Lord, D. Nepomuceno, A. Ahnaou, W. Drinkenburg, W. Chai, C. Dvorak, S. Sands, N. Carruthers, T.W. Lovenberg, Translational Evaluation of JNJ-18038683, a 5-Hydroxytryptamine Type 7 Receptor Antagonist, on Rapid Eye Movement Sleep and in Major Depressive Disorder, J. Pharmacol. Exp. Ther. 342 (2) (2012) 429–440.

[8] H. Alkadi, R. Jbeily, Infectious Disorders - Drug Targets (Formerly 'Current Drug Targets - Infectious Disorders'), Infect. Disord. - Drug Targets. 17 (2017), https://doi.org/10.2174/1871526517666170329123845, 1 1.

[9] Sekhon, Exploiting the Power of Stereochemistry in Drugs: An Overview of Racemic and Enantiopure Drugs, J. Mod Med. Chem. 10–36 (2013), https://doi.org/10.12970/2308-8044.2013.01.01.2.

[10] L. Di, E.H. Kerns, Drug-Like Properties: Concepts, Structure Design and Methods from ADME to Toxicity, Optimization (2015), https://doi.org/10.1016/C2013-0-18378-X.

[11] A. Abelö, T.B. Andersson, M. Antonsson, A.K. Naudot, I. Skånberg, L. Weidolf, Stereoselective metabolism of omeprazole by human cytochrome P450 enzymes, Drug Metab. Dispos. 28 (2000) 966–972 (accessed September 30, 2019), http://www.ncbi.nlm.nih.gov/pubmed/10901708.

[12] H.K. Kroemer, M.F. Fromm, M. Eichelbaum, Stereoselectivity in Drug Metabolism and Action: Effects of Enzyme Inhibition and Induction: Ther. Drug Monit. 18 (4) (1996) 388–392.

[13] A. Gross, A.A. Somogyi, M. Eichelbaum, Stereoselective Drug Metabolism and Drug Interactions., in: Stereochem. Asp. Drug Action Dispos., Springer-Verlag Berlin Heidelberg, 2003: pp. 313–339.

[14] H. Echizen, B. Vogelgesang, M. Eichelbaum, Effects of d,l-verapamil on atrioventricular conduction in relation to its stereoselective first-pass metabolism, Clin. Pharmacol. Ther. 38 (1) (1985) 71–76.

[15] L. Fjordside, U. Jeppesen, C.B. Eap, K. Powell, P. Baumann, K. Brøsen, The stereoselective metabolism of fluoxetine in poor and extensive metabolizers of sparteine, Pharmacogenetics. 9 (1999) 55–60 (accessed September 30, 2019), http://www.ncbi.nlm.nih.gov/pubmed/10208643.

[16] A. Ates, P. Burssens, O. Lorthioir, P. LoBrutto, G. Dehon, J. Keyaerts, F. Coloretti, B. Lallemand, V. Verbois, M. Gillard, C. Vermeiren, 5-HT 7 Receptor Antagonists with an Unprecedented Selectivity Profile, ChemMedChem 13 (8) (2018) 795–802.

[17] V. Grattan, A.R. Vaino, Z. Prensky, M.S. Hixon, Antipsychotic Benzamides Amisulpride and LB-102 Display Polypharmacy as Racemates, S Enantiomers Engage Receptors D 2 and D 3 , while R Enantiomers Engage 5-HT 7, ACS Omega 4 (9) (2019) 14151–14154.

[18] J. Handzlik, A.J. Bojarski, G. Satała, M. Kubacka, B. Sadek, A. Ashoor, A. Siwek, M. Więcek, K. Kucwaj, B. Filipek, K. Kieć-Kononowicz, SAR-studies on the importance of aromatic ring topologies in search for selective 5-HT7 receptor ligands among phenylpiperazine hydantoin derivatives, Eur. J. Med. Chem. 78 (2014) 324–339, https://doi.org/10.1016/j.ejmech.2014.01.065.

[19] K. Kucwaj-Brysz, D. Warszycki, S. Podlewska, J. Witek, K. Witek, A. González Izquierdo, G. Satała, M.I. Loza, A. Lubelska, G. Latacz, A.J. Bojarski, M. Castro, K. Kieć-Kononowicz, J. Handzlik, Rational design in search for 5-phenylhydantoin selective 5-HT7R antagonists. Molecular modeling, synthesis and biological evaluation, Eur. J. Med. Chem. 112 (2016) 258–269, https://doi.org/10.1016/j.ejmech.2016.02.024.

[20] K. Kucwaj-Brysz, R. Kurczab, M. Jastrzębska-Więsek, E. Żesławska, G. Satała, W. Nitek, A. Partyka, A. Siwek, A. Jankowska, A. Wesołowska, K. Kieć-Kononowicz, J. Handzlik, Computer-aided insights into receptor-ligand interaction for novel 5-arylhydantoin derivatives as serotonin 5-HT 7 receptor agents with antidepressant activity, Eur. J. Med. Chem. 147 (2018) 102–114, https://doi.org/10.1016/j.ejmech.2018.01.093.

[21] K. Kucwaj-Brysz, R. Kurczab, E. Żesławska, A. Lubelska, M.A. Marć, G. Latacz, G. Satała, W. Nitek, K. Kieć-Kononowicz, J. Handzlik, The role of aryl-topology in balancing between selective and dual 5-HT 7 R/5-HT 1A actions of 3,5-substituted hydantoins, Med. Chem. Commun. 9 (6) (2018) 1033–1044, https://doi.org/10.1039/c8md00168e.

[22] A. Mangoni, C. Guillou, J. Vanden Eynde, C. Hulme, J. Jampilek, W. Li, K. Prokai-Tatrai, J. Rautio, S. Collina, T. Tuccinardi, M. Sousa, J.-M. Sabatier, S. Galdiero, R. Karaman, G. Kokotos, G. Torri, F. Luque, M. Vasconcelos, D. Hadjipavlou-Litina, C. Siciliano, M. Gütschow, R. Ragno, P. Gomes, L. Agrofoglio, D. Muñoz-Torrero, Breakthroughs in Medicinal Chemistry: New Targets and Mechanisms, New Drugs, New Hopes–4, Molecules. 24 (2018) 130. 10.3390/molecules24010130.

[23] G. Latacz, A. Lubelska, M. Jastrzębska-Więsek, A. Partyka, K. Kucwaj-Brysz, A. Wesołowska, K. Kieć-Kononowicz, J. Handzlik, MF-8, a novel promising arylpiperazine-hydantoin based 5-HT 7 receptor antagonist: In vitro drug-likeness studies and in vivo pharmacological evaluation, Bioorg. Med. Chem. Lett. 28 (2018) 878–883, https://doi.org/10.1016/j.bmcl.2018.02.003.

[24] E. Żesławska, A. Kincses, G. Spengler, W. Nitek, W. Tejchman, J. Handzlik, Pharmacophoric features for a very potent 5-spirofluorenehydantoin inhibitor of cancer efflux pump ABCB1, based on X-ray analysis, Chem. Biol. Drug Des. 93 (2019) 844–853, https://doi.org/10.1111/cbdd.13473.

[25] C.R. Groom, I.J. Bruno, M.P. Lightfoot, S.C. Ward, The Cambridge Structural Database, Acta Crystallogr. B Struct. Sci. Cryst. Eng. Mater. 72 (2) (2016) 171–179, https://doi.org/10.1107/S2052520616003954.

[26] G. Latacz, A. Lubelska, M. Jastrzębska-Więsek, A. Partyka, A. Sobiło, A. Olejarz, K. Kucwaj-Brysz, G. Satała, A.J. Bojarski, A. Wesołowska, K. Kieć-Kononowicz, J. Handzlik, In the search for a lead structure among series of potent and selective hydantoin 5-HT $_7$ R agents: The drug-likeness in vitro study, Chem. Biol. Drug. Des. 90 (6) (2017) 1295–1306.

[27] G. Latacz, A.S. Hogendorf, A. Hogendorf, A. Lubelska, J.M. Wierońska, M. Woźniak, P. Cieślik, K. Kieć-Kononowicz, J. Handzlik, A.J. Bojarski, Search for a 5-CT alternative. In vitro and in vivo evaluation of novel pharmacological tools: 3-(1-

alkyl-1H-imidazol-5-yl)-1H-indole-5-carboxamides, low-basicity 5-HT7 receptor agonists., Medchemcomm. 9 (2018) 1882–1890. 10.1039/c8md00313k.
[28] R.S. Obach, Prediction of Human Clearance of Twenty-Nine Drugs from Hepatic Microsomal Intrinsic Clearance Data: An Examination of In Vitro Half-Life Approach and Nonspecific Binding to Microsomes, Drug Metab. Dispos. 27 (1999) 1350–1359.
[29] A.F. Nassar, P.F. Hollenberg, J. Scatina, Drug metabolism handbook : concepts and applications, Wiley, 2009 (accessed May 24, 2019), https://www.wiley.com/en-af/Drug+Metabolism+Handbook%3A+Concepts+and+Applications-p-9780470118030.
[30] A.A.R. Impellizzeri, M. Pappalardo, L. Basile, O. Manfra, K.W. Andressen, K. A. Krobert, A. Messina, F.O. Levy, S. Guccione, Identification of essential residues for binding and activation in the human 5-HT7(a) serotonin receptor by molecular modeling and site-directed mutagenesis, Front. Behav. Neurosci. 9 (2015) 1–12, https://doi.org/10.3389/fnbeh.2015.00092.
[31] A. Gaulton, L.J. Bellis, A.P. Bento, J. Chambers, M. Davies, A. Hersey, Y. Light, S. McGlinchey, D. Michalovich, B. Al-Lazikani, J.P. Overington, ChEMBL: A large-scale bioactivity database for drug discovery, Nucleic Acids Res. 40 (2012) 1100–1107, https://doi.org/10.1093/nar/gkr777.
[32] Y. Cheng, W.H. Prusoff, Relationship between the inhibition constant (K1) and the concentration of inhibitor which causes 50 per cent inhibition (I50) of an enzymatic reaction, Biochem. Pharmacol. 22 (1973) 3099–3108.
[33] M.C. Burla, R. Caliandro, B. Carrozzini, G.L. Cascarano, C. Cuocci, C. Giacovazzo, M. Mallamo, A. Mazzone, G. Polidori, Crystal structure determination and refinement viaSIR2014, J. Appl. Crystallogr. 48 (1) (2015) 306–309, https://doi.org/10.1107/S1600576715001132.
[34] G.M. Sheldrick, Crystal structure refinement with SHELXL, Acta Crystallogr. C Struct. Chem. 71 (1) (2015) 3–8, https://doi.org/10.1107/S2053229614024218.
[35] C.F. Macrae, P.R. Edgington, P. McCabe, E. Pidcock, G.P. Shields, R. Taylor, M. Towler, J. van de Streek, IUCr, *Mercury* : visualization and analysis of crystal structures, J. Appl. Crystallogr. 39 (2006) 453–457, https://doi.org/10.1107/S002188980600731X.
[36] V.N. Staroverov, G.E. Scuseria, J. Tao, J.P. Perdew, Comparative assessment of a new nonempirical density functional: Molecules and hydrogen-bonded complexes, J. Chem. Phys. 119 (2003) 12129–12137, https://doi.org/10.1063/1.1626543.
[37] F. Weigend, R. Ahlrichs, Balanced basis sets of split valence, triple zeta valence and quadruple zeta valence quality for H to Rn: Design and assessment of accuracy, Phys. Chem. Chem. Phys. 7 (18) (2005) 3297, https://doi.org/10.1039/b508541a.
[38] A.D. Becke, Density-functional thermochemistry. III. The role of exact exchange, J. Chem. Phys. 98 (7) (1993) 5648–5652.
[39] O.A. Vydrov, G.E. Scuseria, Assessment of a long-range corrected hybrid functional, J. Chem. Phys. 125 (2006), 234109, https://doi.org/10.1063/1.2409292.
[40] C. Adamo, V. Barone, Toward reliable density functional methods without adjustable parameters: The PBE0 model, J. Chem. Phys. 110 (13) (1999) 6158–6170.
[41] J. Da Chai, M. Head-Gordon, Long-range corrected hybrid density functionals with damped atom–atom dispersion corrections, Phys. Chem. Chem. Phys. 10 (44) (2008) 6615, https://doi.org/10.1039/b810189b.
[42] P. Śliwa, J. Handzlik, I. Czeluśniak, Alkynol polymerization catalysed by Grubbs-type and Hoveyda–Grubbs ruthenium alkylidene complexes: A computational study, J. Organomet. Chem. 767 (2014) 6–15, https://doi.org/10.1016/j.jorganchem.2014.05.019.
[43] I. Czeluśniak, J. Handzlik, M. Gierada, T. Szymańska-Buzar, Catalytic transformation of phenylacetylene mediated by phosphine-free ruthenium alkylidene complexes, J. Organomet. Chem. 786 (2015) 31–39, https://doi.org/10.1016/j.jorganchem.2015.03.025.
[44] M. Gierada, I. Czeluśniak, J. Handzlik, Terminal-Alkyne-Induced Decomposition of a Phosphine-Free Ruthenium Alkylidene Catalyst, ChemCatChem 9 (12) (2017) 2284–2291.
[45] Y. Zhao, D.G. Truhlar, The M06 suite of density functionals for main group thermochemistry, thermochemical kinetics, noncovalent interactions, excited states, and transition elements: Two new functionals and systematic testing of four M06-class functionals and 12 other functionals, Theor. Chem. Acc. 120 (2008) 215–241, https://doi.org/10.1007/s00214-007-0310-x.
[46] R. Ditchfield, Self-consistent perturbation theory of diamagnetism: I. A gauge-invariant LCAO method for N.M.R. chemical shifts, Mol. Phys. 27 (4) (1974) 789–807.
[47] K. Wolinski, J.F. Hinton, P. Pulay, Efficient implementation of the gauge-independent atomic orbital method for NMR chemical shift calculations, J. Am. Chem. Soc. 112 (23) (1990) 8251–8260.
[48] J. Tomasi, B. Mennucci, R. Cammi, Quantum Mechanical Continuum Solvation Models, Chem. Rev. 105 (8) (2005) 2999–3093.
[49] M.J. Frisch, G.W. Trucks, H.B. Schlegel, G.E. Scuseria, M.A. Robb, J.R. Cheeseman, G. Scalmani, V. Barone, G.A. Petersson, H. Nakatsuji, X. Li, M. Caricato, A.V. Marenich, J. Bloino, B.G. Janesko, R. Gomperts, B. Mennucci, H.P. Hratchian, J.V. et al., Gaussian 16, Revision A.03, (2016) Gaussian, Inc., Wallingford CT.
[50] LigPrep, Schrödinger Release 2018-4, LLC, New York, NY, 2018., (n.d.).
[51] Schrödinger Release 2018-4: Glide, Schrödinger, LLC, New York, NY, 2018., (n.d.).
[52] Schrödinger Release 2018-4: Desmond Molecular Dynamics System, D. E. Shaw Research, New York, NY, 2018. Maestro-Desmond Interoperability Tools, Schrödinger, New York, NY, 2018, (n.d.).
[53] W.L. Jorgensen, J. Chandrasekhar, J.D. Madura, R.W. Impey, M.L. Klein, Comparison of simple potential functions for simulating liquid water, J. Chem. Phys. (1983), https://doi.org/10.1063/1.445869.
[54] J.B. Vaidyanathan, T. Walle, Transport and metabolism of the tea flavonoid (-)-epicatechin by the human intestinal cell line Caco-2, Pharm. Res. 18 (2001) 1420–1425, https://doi.org/10.1023/A:1012200805593.
[55] X. Chen, A. Murawski, K. Patel, C.L. Crespi, P.V. Balimane, A Novel Design of Artificial Membrane for Improving the PAMPA Model, Pharm Res 25 (7) (2008) 1511–1520, https://doi.org/10.1007/s11095-007-9517-8.